Polymer Bulletin
https://doi.org/10.1007/s00289-020-03372-4

ORIGINAL PAPER

Ferroelectric ceramic dispersion to enhance the β phase of polymer for improving dielectric and ferroelectric properties of the composites

Smaranika Dash[1] · Hari Sankar Mohanty[1] · Ravikant[2,3,4] · Ashok Kumar[2,3] · Reji Thomas[5,6] · Dillip K. Pradhan[1]

Received: 20 January 2020 / Revised: 11 June 2020 / Accepted: 18 September 2020

Abstract

Ferroelectric ceramic–polymer composites consisting of Poly Vinyledine Fluoride–Hexa Fluoro Propylene (PVDF-HFP) as polymer host and $0.5Ba(Zr_{0.2}Ti_{0.8})O_3-0.5(Ba_{0.7}Ca_{0.3})TiO_3$ (BZT-BCT) ceramics as filler were prepared using solution casting technique. These composites are characterized for structural, microstructural, vibrational, optical, dielectric and ferroelectric properties at various experimental conditions. The electroactive β phase fraction (observed from XRD and FTIR analysis) increases as the filler concentration increases up to 20 wt% of BZT-BCT and above that its value decreases. FTIR results were analyzed to understand the mechanism of enhancement of β phase by the interaction between negatively surface charged ions of filler with the CH_2 dipole of polymer matrix. UV–visible spectroscopy also employed to confirm polymer–ceramic filler interaction. Variation of the dielectric constant with different filler concentrations is explained using the percolation theory. Finally, the interplay between the functional properties and the β phase is discussed in detail.

Keywords PVDF-HFP · Ferroelectric polymer composite · FTIR · Dielectric properties · Ferroelectric properties

Electronic supplementary material The online version of this article (https://doi.org/10.1007/s00289-020-03372-4) contains supplementary material, which is available to authorized users.

✉ Dillip K. Pradhan
dillip.pradhan79@gmail.com

Extended author information available on the last page of the article

Published online: 30 September 2020

Introduction

Ferroelectric materials have been widely used in various devices such as non-volatile random access memory, sensors, actuators, transducers and high energy density capacitors, due to its excellent dielectric, ferroelectric and piezoelectric properties [1, 2]. However, in ceramic form, high dielectric constant (ε_r) of these materials is less exploited in related devices due to the lack of design flexibility arisen from the brittle nature, low elasticity and small dielectric breakdown strength. These latter mentioned drawbacks prevent its application in high energy density capacitors [3], an excellent energy storage device of contemporary importance. Contrary to this, polymers show better mechanical strength, good flexibility and high dielectric break down strength [4]. However, the major drawback of polymer is the low dielectric constant, a pre-requisite for realizing high energy density [3, 4]. So, by combining both ceramic and polymer, resulting ceramic-polymer composite is expected to show higher breakdown strength, flexibility as compared to the ceramics and high dielectric constant compared to polymer. Therefore, ceramic–polymer composites are the focus of the current research in high density energy storage devices. Recently, ceramic–polymer composites have also explored in various practical application such as, in optoelectronics, transistor, embedded capacitors, energy harvesting and biomaterials in biomedical field [5]. To get a flexible ceramic–polymer composite with optimum properties, mixing of polymer matrix with ceramic filler in a proper ratio is the key factor. Generally, for the fabrication of polymer composites, three important factors must be taken into account such as (1) a polymer matrix having high dielectric constant with low loss, (2) a suitable preparation technique to ensure uniform distribution of ceramic fillers into the polymer matrix [6] and (3) the interface of different phase in polymer composites which mainly depend on the chemical structure of both polymer matrix and filler [7]. Poly (Vinyledine fluoride) (PVDF) and its copolymer such as Poly(Vinyledine fluoride-chlorotrifluroethylene) P(VDF-CTFE), Poly(Vinyledine fluoride-tetrafluroethylene) P(VDF-TFE), Poly(Vinyledine fluoride-trifluroethylene) P(VDF-TrFE), Poly (Vinyledine fluoride-cohexafluoropropylene) (PVDF-HFP) are some of the widely used polymers due to their high dielectric constant [8, 9]. As can be seen, in all these materials PVDF is paired with its copolymer. PVDF is an electroactive polymer, semi-crystalline in nature with dielectric, ferroelectric, piezoelectric and pyroelectric properties [10]. Generally, copolymers are added to PVDF to improve/tailor the physical properties targeted for the particular application [5]. For example, addition of monomers like hexafluoropropylene (HFP) into the PVDF chain improves dielectric properties, but reduces crystallinity (due to the presence of CF_3 group) [5]. The chemical stability with improved dielectric properties of PVDF-HFP is promising for optoelectronics devices, sensors and super capacitors [11, 12]. In fact, PVDF-HFP exists in different phases, α, β, γ, δ and ε, depending upon the arrangement of monomer unit ($–CH_2–CF_2$) as in the case of pure PVDF [13]. α is the nonpolar phase which is characterized by trans-gauge-trans-gauge (TGTG′) order of the polymeric chain. However, β phase is the important one which is

polar in nature with trans–trans-trans–trans (TTTT) order while γ and ε has the same order TTTGTTTG′ [14]. In β phase, H and F are arranged in opposite direction gives rise to a nonzero dipole moment responsible for the ferroelectric and piezoelectric properties [15]. Hence, the enhancement of electro-active β phase in PVDF-HFP polymer and its composite has received a great interest. To enhance the β phase, different techniques such as mechanical stretching of α phase at a suitable temperature [16], electrical poling [17], γ-ray irradiation [18] and electrospinning [19] have been successfully employed. Recently, addition of various fillers such as semiconductor nano-particles (ZnO, TiO_2, GeO_2, SiO_2), carbon-based (Carbon nanotube and graphene) and clay-based (Montmorillonite (MMT)) filler to the aforementioned polymer matrix has also been used to enhance the β phase [12, 13, 20–22]. The dispersion of the aforementioned fillers into the polymer matrix increases ε_r up to a certain concentration known as percolation threshold and further increase in filler concentration reduces ε_r [23, 24]. But such composite has some drawback, i.e., high dielectric loss (tanδ) and low dielectric breakdown strength (E_{BD}) which restricts its application in embedded capacitor [8]. In this context, addition of perovskite-based ceramics ($PbTiO_3$, $Pb(ZrTi)O_3$, $K_{0.5}Na_{0.5}NbO_3$ and $BaTiO_3$) into the polymer matrix is one of the suitable approaches to overcome the drawback as these materials invariably have high dielectric constant [25].

Based on the above discussion, the fractional improvement of β phase in the polymer directly enhances the physical properties which is essential from application point of view. Ceramic–polymer composite with ferroelectric ceramic filler is one of the ways to enhance the β phase of the polymer. Various methods such as solution casting, tape casting, hot pressing and compression molding were generally used for preparing the polymer composite in different size and shapes [24, 26]. Solution casting technique has several advantages over other technique as it is easy to fabricate thin/thick and small/large film [27]. Out of different ferroelectric ceramics, barium titanate (BT) is widely used in the energy storage devices because of high ε_r, non-toxicity, and environmental benevolence. Recently, Ca^{2+} and Zr^{4+} modified BT-based material, i.e., $0.5\ Ba(Zr_{0.2}Ti_{0.8})O_3-0.5(Ba_{0.7}Ca_{0.3})TiO_3$ (BZT-BCT), also considered as the morphotropic boundary (MPB) composition, has enhanced dielectric, ferroelectric and piezoelectric properties [28]. Polymer composites using BZT-BCT and PVDF showed high dielectric constant value of 100 for 61 wt% of BZT-BCT at 1 kHz with a loss value nearly 0.01 [25]. However, 25 wt% of BZT-BCT composite showed a dielectric constant of 44 with a loss of 0.02 at 1 kHz [29]. Also, in copolymer added PVDF (PVDF-HFP)–(BZT-BCT) composite, ε_r and tanδ were 19 and 0.08, respectively, at 10 kHz for 15 wt% of BZT-BCT [30]. Reported results are not comparable as frequency or the filler concentration varying in each cases. Although BZT-BCT-based polymer composite has been studied based on the effect of filler concentration on dielectric properties, but no detailed studies have been reported for the enhancement of β phase with different concentration of BZT-BCT and its correlation with the physical properties. In view of this, present communication considers ferroelectric ceramic (BZT-BCT) based polymer (PVDF-HFP) composites and the influence of filler concentration on various properties; β-phase enhancement and the mechanism of enhancement.

Experimental procedure

Synthesis of (PVDF-HFP)–(BZT-BCT) composite

Auto-combustion and solution casting technique were used for the preparation of ceramic and polymer composite films, respectively. Polycrystalline lead-free $0.5Ba(Zr_{0.2}Ti_{0.8})O_3-0.5(Ba_{0.7}Ca_{0.3})TiO_3$ (BZT-BCT) ceramic powder was synthesized first using auto-combustion technique by maintaining fuel (F) to oxidizer (O) ratio 1. For this, stoichiometry amount of $Ba(NO_3)_2$ (99% Alfa aesar), $Ca(NO_3)_2.4H_2O$ (99% Alfa aesar), $ZrO(NO_3)_2.xH_2O$ (99% Sigma-Aldrich), Ti $[OCH(CH_3)_2]_4$ (97% Alfa aesar) and urea (Himedia) were taken and mixed in distilled water. The detailed procedure of the synthesis technique is reported elsewhere [31]. The samples were calcined at 900°C for 6 h and further pressed into pellet which is sintered at 1450°C for 4 h. The prepared pellets were crushed into powder which is further used for the synthesis of composites.

The pure matrix PVDF-HFP and its polymer composites with different wt% of BZT-BCT , *i.e.,* PVDF-HFP + ϕ wt% BZT-BCT, ϕ = 0, 5, 10, 15, 20, 25, 30, 40 were prepared using solution casting technique. For that, 1 gm of PVDF-HFP (> 99%, Sigma-Aldrich) was dissolved in 25 ml of *N*,*N*-dimethylformamide (DMF, Merck) at room temperature using a magnetic stirrer. DMF acts as a polar solvent and dissolved PVDF-HFP at room temperature. The solution was stirred until PVDF-HFP completely dissolved in DMF. Then, different wt% of BZT-BCT were mixed in the solution and stirred continuously overnight at room temperature which is further sonicated for ½ an hour to get homogeneous dispersion of BZT-BCT particles in the solution. The solution was casted in petri dish and dried in an oven at 90 °C for 9 h. for complete evaporation of solvent to get the flexible composite films. The free-standing films prepared this way had a thickness ~ 80 µm. Details of the synthesis procedure is schematically shown in Fig. 1.

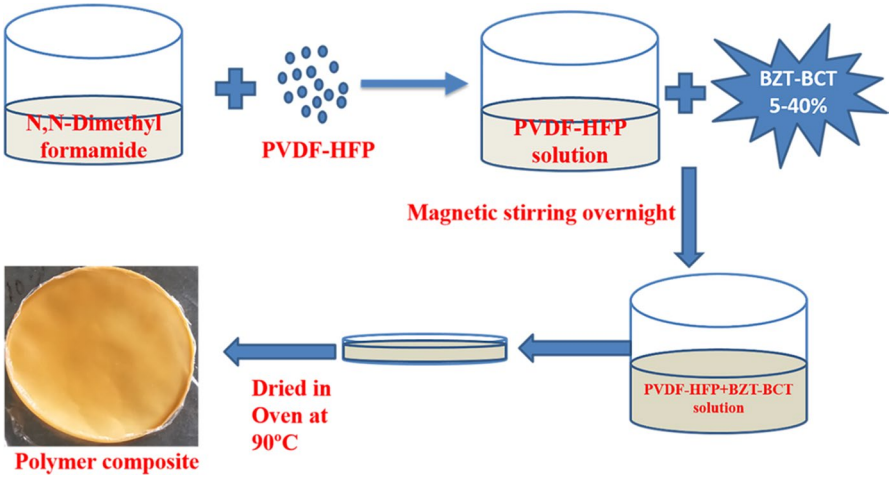

Fig. 1 (Color online) Flowchart for the preparation of pure polymer and polymer composite films

Characterization

The formation and preliminary structural analysis of PVDF-HFP and its polymer composites were examined by X-ray diffractometer (XRD, RIGAKU JAPAN ULTIMA-IV) with Cu $K_{\alpha 1}$ radiation ($\lambda = 1.5405$Å). The data were taken with 2θ values ranging from 5° to 50° at a scan speed of 2°/min. with a step size of 0.05° at room temperature. Surface morphological analysis of composites was performed using SEM (SEM-JEOL-JSM 6480 LV) technique. All the samples were coated with a fine layer of platinum under a vacuum chamber in order to capture the microscopic images of different magnification of the samples. The elemental composition of the film was analyzed by energy-dispersive X-ray (EDS) spectrum. UV visible spectrophotometer (Jasco V-650 with $BaSO_4$ coated integration sphere) was used to study the absorption spectra of the pure PVDF-HFP and PVDF-HFP composite films in the wavelength range 200–800 nm. Fourier transform infrared (FTIR) spectra of all the films were recorded by an IRAFFINITY-1S, Shimadzu spectrometer in the wavenumber range of 400–4000 cm^{-1} with a resolution of 2 cm^{-1}. The surface charge potential of the ceramic filler was studied using Zeta potential analyzer (NanoZS90). The dielectric properties of PVDF-HFP-based composites were examined in the temperature range from 30 °C to 150 °C with a wide range of frequency from 100 Hz to 1 MHz using an impedance analyzer (HIOKI IM3570). The composite films are kept in between two stainless steel electrodes which is further placed in the sample holder to perform the dielectric measurement. The room temperature ferroelectric properties of the composites were studied by Ferroelectric loop tester (Radiant Ferroelectric Tester) at a frequency of 10 Hz.

Results and discussion

Structural and microstructural studies

Figure 2 shows the room temperature XRD pattern of BZT-BCT, PVDF-HFP and PVDF-HFP-based polymer composite with different wt% of BZT-BCT ($\phi = 5\%$, 10%, 15%, 20%, 25%, 30%, 40%). In the diffraction pattern of BZT-BCT ceramic, the characteristic diffraction peaks appear at $2\theta = 22.12°$, 31.47°, 39.04°, 45.25°, which matched with the literature and that confirms the formation of a single-phase material [32, 33]. The XRD pattern of PVDF-HFP consists of crystalline peaks with a broad background hump which suggest the semi-crystalline nature. Also, in the figure, characteristics reflections of polymer (PVDF-HFP) and filler (BZT-BCT) are clearly visible in the composite, suggesting BZT-BCT is uniformly dispersed in PVDF-HFP. This result clearly confirms the formation of polymer composite. In the case of pure PVDF-HFP, diffraction peak observed at $2\theta = 18.3°$(020) represent the nonpolar α phase while the peak at 20.12° (110/200) corresponds to β phase [9, 34]. The reflection at $2\theta = 26.7°$ (021) is associated with α phase [13]. As the BZT-BCT concentration increases, gradual changes were observed in the position, intensity and width of the diffraction peaks. With the increase in filler concentration, the intensity of the β phase (20.12°) increases up to 20 wt% with the reduction

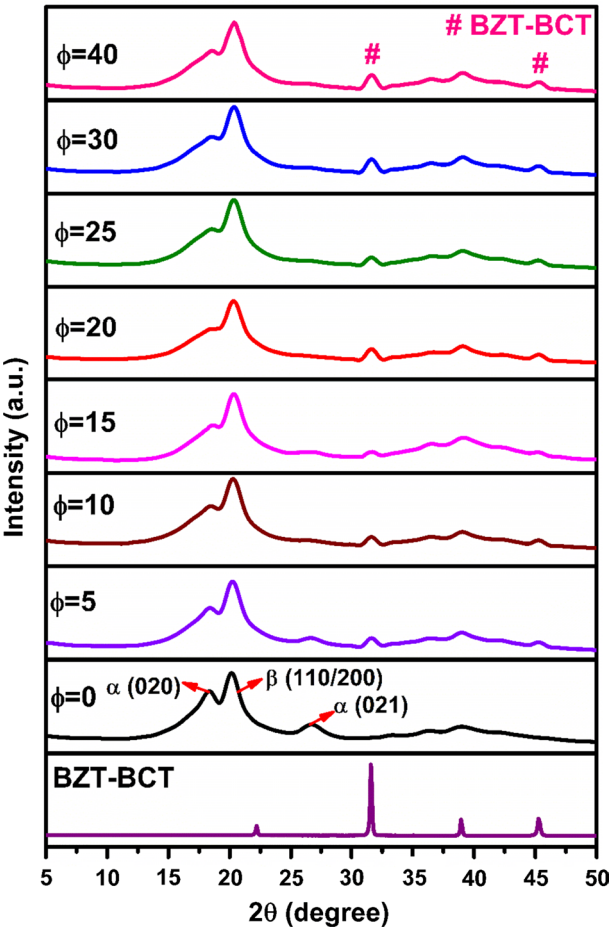

Fig. 2 (Color online) Room temperature XRD patterns of PVDF-HFP + ϕ wt% BZT-BCT polymer composites (ϕ = 0, 5, 10, 15, 20, 25, 30, 40)

in the intensity of α phase (18.3°). Further increase in BZT-BCT concentration, the trend reverses, the intensity of β phase reduces and that of α phase increases. Also, as expected the intensity of the peak at 31.55°, 45.25° (most intense peak of BZT-BCT) increases with the increase in filler concentration as can be seen in Fig. 2. The intensity ratio of β phase w.r.t. α phase ($I^{\circ}_{20.12}/I^{\circ}_{18.3}$) (ordering parameter) of PVDF-HFP and its composite has been calculated from XRD pattern. It is observed that this ratio increases with the increase in the BZT-BCT concentration up to 20 wt% and above that it decreases (see in Fig. 9).

Crystallinity in a composite is one of the important physical parameters as it gives the information about the texture and strength [35]. The polarization of the material also depends on the crystallinity and processing condition [36]. The degree of crystallinity of the films was calculated by deconvoluting the XRD pattern into

crystalline and amorphous peaks (provided in supplementary fig. S1) using the following Eq. (1) [9]

$$\chi_c = \frac{\sum A_{\mathrm{cr}}}{\sum A_{\mathrm{cr}} + \sum A_{\mathrm{amr}}} \times 100 \tag{1}$$

where $\sum A_{\mathrm{cr}}$ and $\sum A_{\mathrm{amr}}$ represent the integrated areas of the crystalline and amorphous region, respectively, in the diffraction pattern. It is observed that the crystallinity of host matrix (PVDF-HFP) is found to be around 31.3% which is well matched with previous reported value, i.e., 33.2% [12]. However, with the increase in concentration of BZT-BCT in PVDF-HFP, the crystallinity of the composite increases up to 20 wt% filler concentration and found to be around 40.2%. However, further increase in the filler concentration crystallinity decreases and will be discussed in a latter section (Fig. 9).

The SEM micrographs of pure PVDF-HFP and composites with different wt% of BZT-BCT are shown in Fig. 3. The micrograph of the pure PVDF-HFP matrix is found to be smooth and continuous suggesting the spherulites, semi-crystalline region in the polymers [13]. Spherulites are existing in spherical shape and made up of ordered lamellae which are connected by amorphous region [37]. As the BZT-BCT particles added to the PVDF-HFP matrix, the distinct spherulites are observed. The formation of spherulites depends on several factors such as structure of polymer molecules, number of nucleation sites and synthesis condition [38]. With the

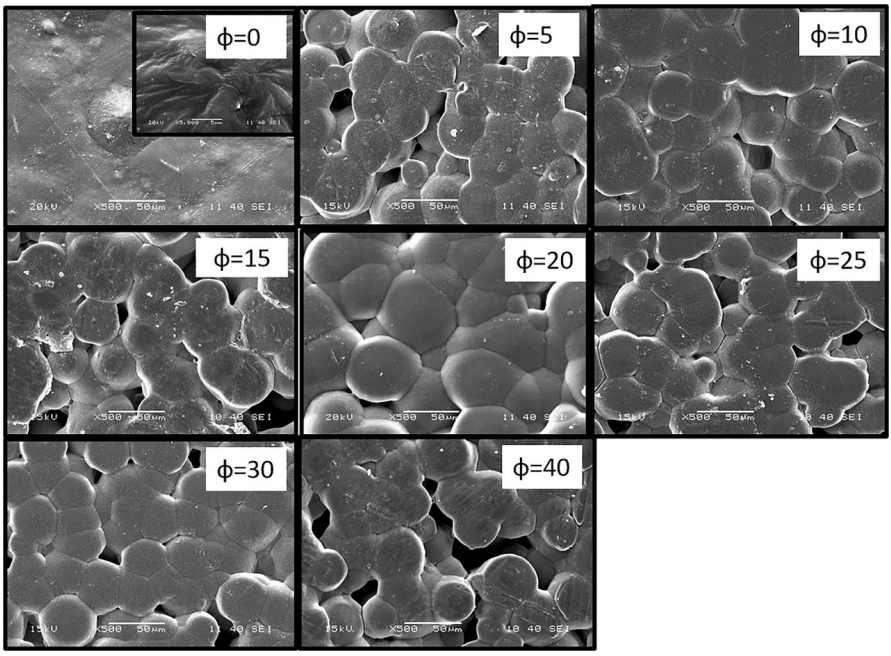

Fig. 3 (Color online) SEM micrographs of PVDF-HFP + ϕ wt% BZT-BCT polymer composites (ϕ = 0, 5, 10, 15, 20, 25, 30, 40)

increase in filler concentration, the spherulites interact with each other and finally merged to form larger spherulites. In the present case, spherulites for 20 wt% BZT-BCT are largest and the size reduced for higher concentrations. This observation implies that BZT-BCT particles act as a nucleation center for the growth of spherulites, and there is an optimum concentration (20%) [39]. Above 20 wt%, its size decreases and porosity also is formed. BZT-BCT particles are uniformly dispersed in the polymer matrix and that indicates the successful synthesis of polymer composite using solution casting technique. The elemental composition of pure polymer (PVDF-HFP) and its polymer composite has been studied from EDX result (given in supplementary fig. S2). EDX spectra of neat PVDF-HFP show the elements like carbon (C), fluorine (F) and oxygen (O). However, for polymer composite, along with the aforementioned elements, barium (Ba), calcium (Ca), zirconium (Zr), titanium (Ti) are also present.

Spectroscopic studies

To understand the interaction of filler with polymer matrix and the band gap of the composites, UV–visible absorption spectra were recorded. Figure 4 shows the absorption spectra of pure polymer (PVDF-HFP) and different wt% of BZT-BCT loaded polymer composite in the wavelength range of 200-800 nm. No absorbance peak is observed for the host polymer matrix suggesting the film is transparent to UV–visible light [40]. For BZT-BCT ceramic, a broad peak is observed around 330.18 nm which is well matched with the previously reported value [41]. This signifies that around this wavelength the absorption process occurs in which electrons excited from lower to higher energy state and it leads to an absorption edge. As the volume fraction of BZT-BCT fillers increases in the composite, the intensity of absorption peak increases and shifted toward lower wavelength. Absorption is observed at 322 nm for the 20 wt% BZT-BCT composites, a shift of 8 nm as compared to pure BZT-BCT (330.18 nm). This is due to the strong electrostatic interaction between BZT-BCT filler and PVDF-HFP polymer chain, which affect the transition between valence band and conduction band of BZT-BCT ceramics [13, 42]. This suggests that the interaction occurs between the polymer matrix and filler in the composite.

The optical energy band gap (E_g) of the polymers and its composites can be calculated by Tauc's model [43] using the following relation

$$\alpha h\nu = B\left(h\nu - E_g\right)^{\gamma} \tag{2}$$

where $h\nu$ is the energy of the incident photon, B is a constant, depending on the transition probability within the optical frequency region. E_g is the optical band gap of the material in eV, α is the absorption coefficient. The index γ gives the information about the nature of electronic transition in the material. The value of γ is ½ and 2 for direct and indirect allowed transition, respectively, while that for the direct and indirect forbidden transition its value are 3/2 and 3, respectively [44]. In the present work, the indirect allowed transition has been considered [44] to find out the band gap (E_g) of the material. The band gap of the pure polymer and its composites has

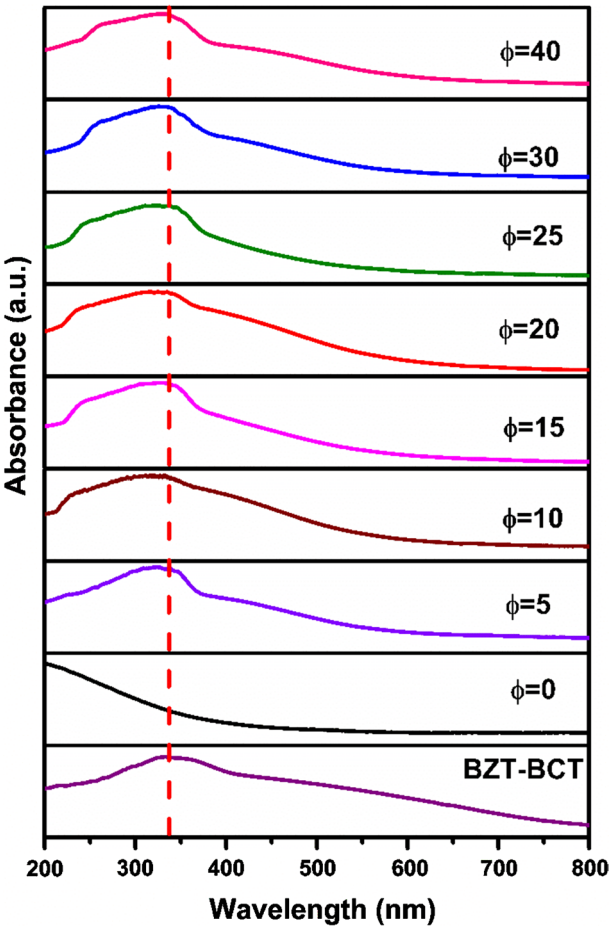

Fig. 4 (Color online) UV Visible absorbance spectra of PVDF-HFP + ϕ wt% BZT-BCT polymer composites (ϕ = 0, 5, 10, 15, 20, 25, 30, 40)

been calculated using Eq. (2) by taking γ = 2 which is shown in fig. S3. By extrapolating the linear portion of the absorption edge on the X-axis, the value of band gap value (E_g) is determined. The value of E_g for PVDF-HFP is found to be around 2.7 eV. However, for BZT-BCT ceramic the band gap value is found to be around 3.04 eV which is close to the value reported elsewhere [45]. With the increase in filler concentration, the optical band gap increases to 3.12 eV for 20 wt% of BZT-BCT composite. The effective optical band gap of a material also depends on the intermediate energy in the actual band gap between the valence and conduction bands [45]. However, the position of such levels depends on the impurities, preparation technique, processing parameters [46]. With the increase in filler concentration, the band gap (E_g) of the composites increases as shown in fig. S3 (provided in supplementary material). As BZT-BCT concentration increases, the intermediate

energy level present between valence band and conduction band decreases and it leads to an increasing value of E_g [47].

Vibrational spectra through Fourier transform infrared spectroscopy (FTIR) are also useful to understand the interaction of filler with the polymer matrix. FTIR spectra of pure polymer and different wt% of BZT-BCT filled PVDF-HFP composites are shown in Fig. 5 in the wavenumber range of 400–1400 cm^{-1}. We have normalized the FTIR data based on the absorption peak present at 878 cm^{-1} in order to compensate the differences in the thicknesses of the samples [48]. In the FTIR spectra of pure PVDF-HFP, the presence of peaks at 493 cm^{-1} (bending vibration of CF_2 group), 538 cm^{-1} (wagging vibration of CF_2 group), 619 cm^{-1} (CF_2 and –C–C–C skeletal vibration), 769 cm^{-1} (CH_2 rocking vibration), 803 cm^{-1} (–CF_3 stretching vibration), 980 cm^{-1} (C–F stretching vibration) is assigned to the non-electroactive α phase [49]. On the other hand, the vibrational bands at 840 cm^{-1} attributed to the

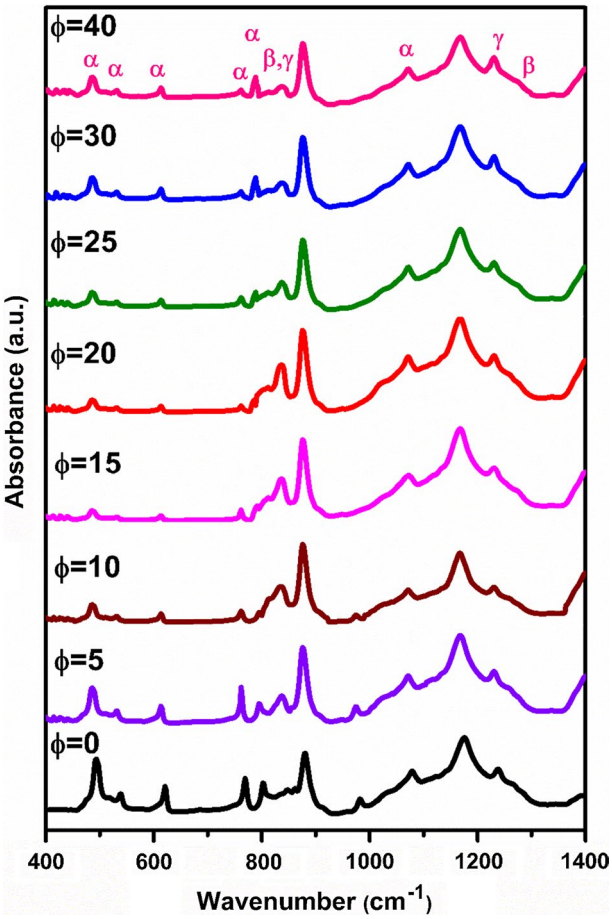

Fig. 5 (Color online) FTIR spectra of PVDF-HFP + ϕ wt% BZT-BCT polymer composites (ϕ = 0, 5, 10, 15, 20, 25, 30, 40) in the wavenumber range of 400–1400 cm^{-1}

polar β phase which corresponds to the mixed CH_2 rocking modes [13]. However, two peaks appear around 1237 cm^{-1} and 1281 cm^{-1} which are characteristic of γ and β phase, respectively [14]. The peak around 1176 cm^{-1} arises due to the symmetric stretching of –C–C–C-bond [49]. These bands are well matched with the previous reported value and summarized in Table S1. From Fig. 5, it has been observed that for pure (PVDF-HFP) matrix, the intensity of β phase (peak around 840 cm^{-1}) is very less as compared to α phase (peak around 769 cm^{-1}). As BZT-BCT incorporated into PVDF-HFP, changes occur in the position of the band and its intensity. In the polymer composite, the intensity of β phase increases with the decrease in the intensity of α phase up to 20 wt% of BZT-BCT and above that the trend reverses. This changes in the fraction of β phase ($F(\beta)\%$) content with respect to α phase from FTIR spectra were calculated using Lambert–Beer Law [13], i.e.,

$$F(\beta) = \frac{A_\beta}{\left(K_\beta / K_\alpha\right) A_\alpha + A_\beta} \tag{3}$$

where A_α and A_β are the absorption value at the wavenumbers 769 cm^{-1} and 840 cm^{-1}, respectively, while K_α and K_β are the absorption coefficient at the respective wavenumbers whose values are 6.1×10^4 cm^2 mol^{-1} and 7.7×10^4 cm^2 mol^{-1}. The $F(\beta)$ % value for pure matrix and its polymer composites with different wt% of BZT-BCT are shown in Fig. 9. For pure PVDF-HFP, the fraction of β phase is found to be 34% while with the increase in BZT-BCT concentration its value increases up to 20 wt% of BZT-BCT, i.e., 68% and above it, its value decreases. With the increase in the filler concentration, the interaction between the polymer matrix and filler increases which results in the enhancement of β phase. This concludes the enhancement of β phase up to 20 wt% and is well matched with the XRD result discussed earlier.

The enhancement of β phase is further explained by dipole-surface charge interaction between PVDF-HFP and BZT-BCT, respectively. In order to study this interaction in the polymer composite, FTIR spectra of the composites were plotted in the wavenumber region of 2950–3050 cm^{-1} and are shown in Fig. 6a. This region is mainly associated with the symmetric ν_s ($–CH_2$) and antisymmetric ν_{as} ($–CH_2$) stretching vibrational band, and they are not coupled with any other vibrational band [14]. This region is very important to check whether there is any interfacial interaction taking place between the $–CH_2$ dipoles of PVDF-HFP with the BZT-BCT filler. From Fig. 6a, it has been observed that, with the increase in filler concentration the position of ν_s ($–CH_2$) and ν_{as} ($–CH_2$) band shifts toward the lower wavenumber side indicating the interaction between BZT-BCT and PVDF-HFP. The shifting of these bands toward lower wavenumber with the increase in BZT-BCT concentration up to 20 wt% and above that the shifting toward higher wavenumber has also been observed. This gives a piece evidence for the interaction which takes place between surface charges of BZT-BCT with PVDF-HFP matrix. We have performed the Zeta potential experiment to check whether the surface of filler (BZT-BCT) is positively or negatively charged. Figure S4 shows the Zeta potential distribution of BZT-BCT filler. The surface charge of BZT-BCT filler is found to be negative with a Zeta potential value of − 18.9 mV. The interaction between negatively charged

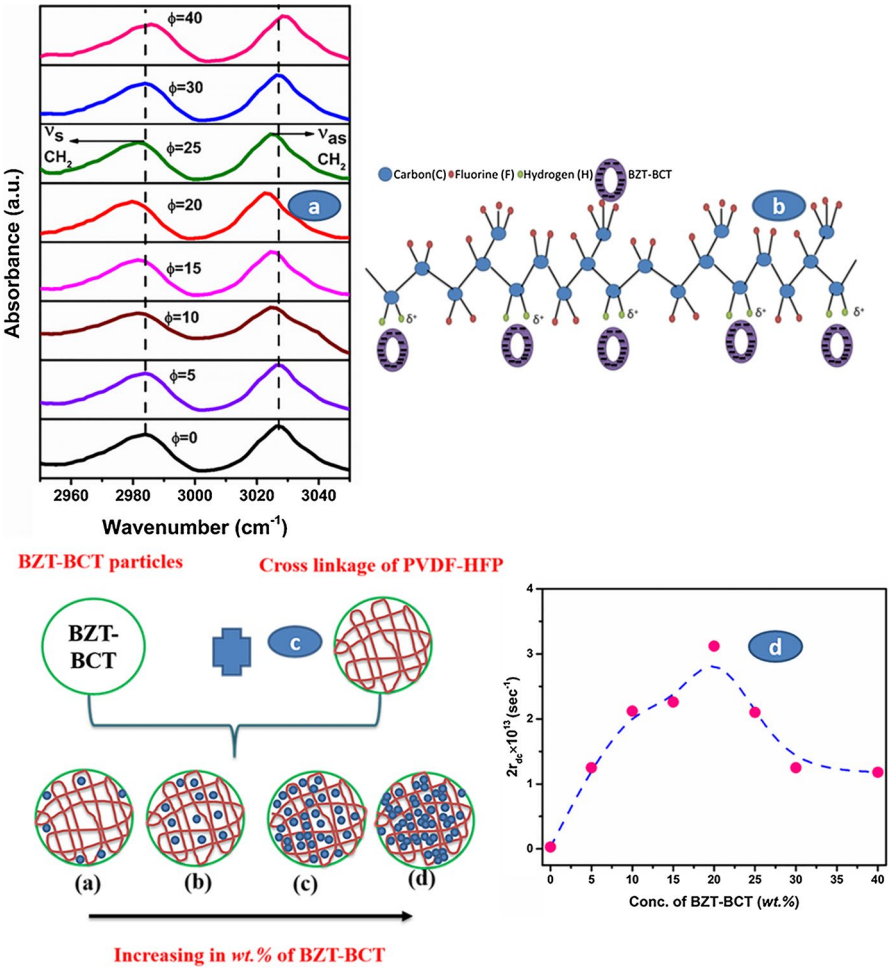

Fig. 6 (Color online) **a** FTIR absorbance spectra of PVDF-HFP + ϕ wt% BZT-BCT polymer composites (ϕ = 0, 5, 10, 15, 20, 25, 30, 40) in the wavenumber range of 2950–3050 cm^{-1} **b** Interaction between –CH$_2$ dipole of polymer (PVDF-HFP) and negatively surface charge of filler (BZT-BCT) **c** Schematic diagram of loading of different concentration of BZT-BCT filler into PVDF-HFP polymer chain with an increasing wt% of BZT-BCT **d** Variation of $2r_{dc}$ with different wt% of BZT-BCT

surfaces of BZT-BCT with the -CH$_2$ dipoles of PVDF-HFP is represented in a schematic diagram as shown in Fig. 6b. At lower concentration of filler, weak interaction occurs between the negative surface charge of BZT-BCT filler and partially positively charged of –CH$_2$ dipole of the PVDF-HFP matrix. As the filler concentration increases, the negatively charged filler interacts strongly with the partially positively charged –CH$_2$ dipoles of PVDF-HFP results in the straightening of chain. This resulted in the increment of TTTT confirmation in PVDF-HFP polymer chain leads to an enhancement of β phase. This negatively charged BZT-BCT acts as a nucleation agent for the enhancement of β phase [14]. At higher concentration of fillers,

the particles may get agglomerated as shown in Fig. 6c in the PVDF-HFP matrix and it further opposes the nucleation process results a decrease in the electroactive phase formation in the polymer.

The interaction between the $–CH_2$ dipoles and the charge distributed on the surface of BZT-BCT act as a damping source for the oscillation of $–CH_2$ dipole results a shifting of vibrational band toward lower energy (lower wavenumber) region. This phenomenon can be well explained by the damped harmonic oscillation of $–CH_2$ dipole [50], i.e.,

$$r_{dc} = 2\pi c\left(\bar{\nu}_0^2 - \bar{\nu}^2\right)^{1/2} \tag{4}$$

where r_{dc} is the damping coefficient, $\bar{\nu}_0$ represents the wavenumber of $–CH_2$ free damping vibration of PVDF-HFP and $\bar{\nu}$ is the damped vibration of BZT-BCT in PVDF-HFP film and c is the speed of light [14]. Figure 6d shows the variation of $2r_{dc}$ (damping constant) with different concentration of BZT-BCT. It has been observed that the $2r_{dc}$ value increases with the increase in filler concentration up to 20 wt% of BZT-BCT and the value decreases after that. r_{dc} is a physical parameter from which the information about electroactive phase formation can be extracted due to the strong electrostatic interaction between $–CH_2$ dipole of PVDF-HFP and negatively surface charged ion of BZT-BCT. The behavior of β phase fraction (Fig. 9) and damping constant (Fig. 6d) with BZT-BCT concentrations shows similar type of behavior. This confirms the enhancement of electroactive β phase observed up to 20 wt% due to the strong interaction between negatively surface charged of BZT-BCT and $–CH_2$ dipole of PVDF-HFP, which may leads to an enhanced value of dielectric/ferroelectric properties and will be discussed in the following section.

Electrical properties

To study the ferroelectric properties, room temperature hysteresis loop (*P–E*) of neat PVDF-HFP and composites is plotted as shown in Fig. 7a,b at a frequency of

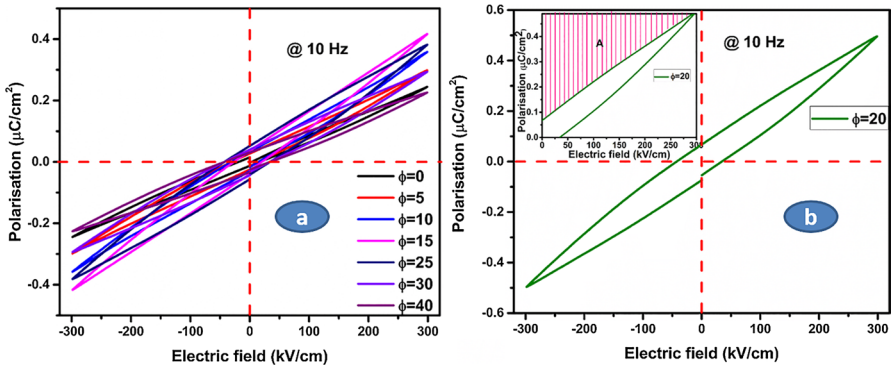

Fig. 7 (Color online) **a** Room temperature hysteresis loop (P–E) of PVDF-HFP + ϕ wt% BZT-BCT polymer composites (ϕ = 0, 5, 10, 15, 25, 30, 40) **b** P–E loop of polymer composite for 20 wt% of BZT-BCT

10 Hz. Before performing this experiment, the films were coated with silver paint. An unsaturated loop has been observed for pure PVDF-HFP due to the application of low voltage (unit not equipped with high voltage to address the coercive field). Even though it is inappropriate to say that saturation of ferroelectric polarization is reached within experimental limitation, a trend has been observed in the P-E hysteresis loop. In this case, we say the highest polarization obtained is P_s. For pure PVDF-HFP, a lower value of saturation polarization (P_s) of 0.25μC/cm^2 is observed. However, with the increase in filler concentration, P_s value increases up to 0.5 μC/cm^2 for 20 wt% BZT-BCT due to the increase in crystallinity and electroactive β phase fraction [36]. Above 20 wt% of BZT-BCT, the P_s value decreases because the agglomeration of particle occurs results in the degradation of ferroelectric properties [51]. This changes in polarization (P_s) value with different wt% of BZT-BCT are discussed in next section. The energy storage density (J) of pure polymer and its composite can be calculated from P-E loop using relation $J = \int E \, dP$; where E is the electric field and P is the polarization [51]. The shaded region in the inset of Fig. 7b represents the energy stored in the material. A higher value of energy storage density is required for high energy density capacitor applications. The value of the calculated storage energy density of the composites loaded with different BZT-BCT concentrations are summarized in Table S2. For pure PVDF-HFP, the storage energy density is found to be 36.08 mJ/cm^3, however, with the increase in the filler concentration it increases up to 20 wt% of BZT-BCT. Above this filler concentrations, its value decreases. The highest value of storage energy density (J) found to be 86.85 mJ/cm^3 at an applied electric field of 300 kV/cm which is comparable to BT/PVDF-HFP-based composite [52]. This enhancement in the storage density is due to the increasing value of dielectric constant due to filler additions.

Dielectric properties, in terms of the dielectric constant (ε_r) and dielectric loss (tanδ) as a function frequency is studied and is shown in Fig. 8a, b for neat PVDF-HFP and its polymers composite at room temperature. A decrease in dielectric constant with the increase in frequency is the typical behavior for a polar dielectric material, which has been observed for both PVDF-HFP and its polymer composite as shown in Fig. 8a. At lower frequency region, especially in the range of 10^2–10^4 Hz, the dielectric constant of neat polymer and its composite with different wt% of BZT-BCT shows a higher value. However, at higher frequency region of 10^4–10^6 Hz, a nearly same dielectric constant value is observed for all the films which is frequency independent. With the increase in filler concentration, the dielectric constant (ε_r) increases up to 20 wt% of BZT-BCT and above that its value decreases. Similarly, in the lower frequency range, the dielectric loss value decreases with the increase in frequency for pure PVDF-HFP matrix and its composite with different wt% of BZT-BCT. The dielectric loss (tanδ) curve shows similar trend as dielectric constant, i.e., its value increases with the increase in BZT-BCT concentration up to 20 wt% and above that it decreases as shown in Fig. 8b. Figure 8c show the variation of dielectric constant and tangent loss with different filler concentration at a frequency of 500 Hz. The dielectric constant and tangent loss value of PVDF-HFP are found to be around 7 and 0.07, respectively, at a frequency of 500 Hz. However, the dielectric constant increases with the increase in filler concentration and a ε_r value of 21 is observed for 20 wt% and above that it starts to decrease. The dielectric constant

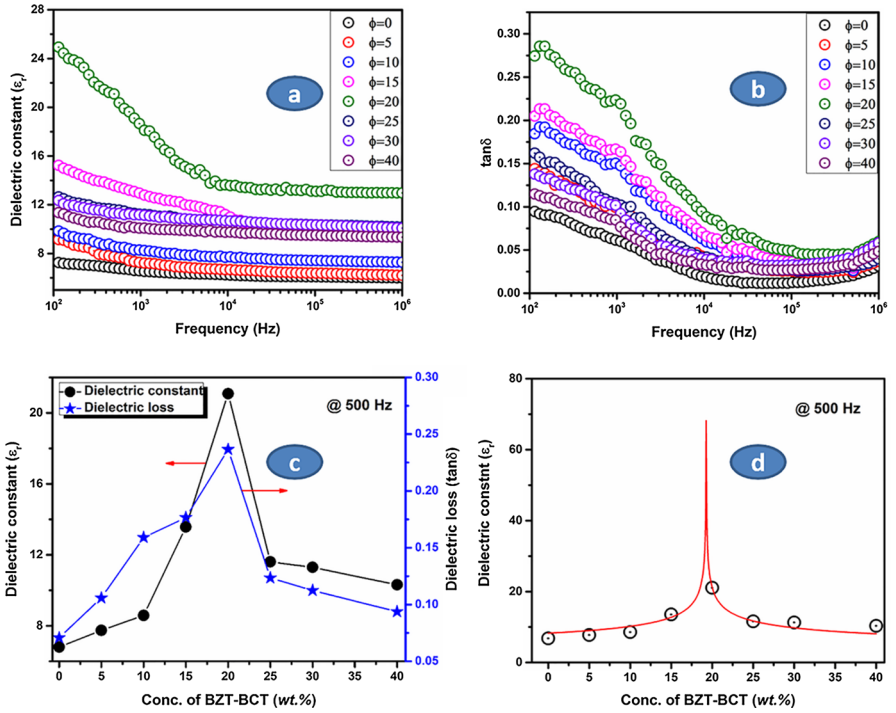

Fig. 8 (Color online) Variation of **a** dielectric constant (ε_r) **b** tangent loss (tanδ) of PVDF-HFP + ϕ wt% BZT-BCT polymer composites (ϕ = 0, 5, 10, 15, 20, 25, 30, 40) as a function of frequency measured at room temperature **c** Variation of ε_r and tanδ with different wt% of BZT-BCT at 500 Hz **d** Fitting of dielectric constant using percolation theory

of 20 wt% BZT-BCT is 3 times higher than that of the pure polymer matrix. The increase in loss value with the increase in filler concentration is due to the formation of conducting network and increase in defects [23]. At lower concentration, the inter particle distance between filler is high results a weak interaction between filler and polymer matrix which leads to a lower dielectric constant value. However, with the increase in filler concentration, ε_r increases up to 20 wt% BZT-BCT due to the increase in interaction between filler and matrix results in the enhancement of β phase (observed from FTIR and XRD) [14]. At higher filler concentration, i.e., above 20 wt%, agglomeration of fillers occurs (shown in Fig. 6c) and that results in the degradation of β phase which leads to decrease in ε_r value as observed in Fig. 9. These changes in dielectric behavior of polymer composites with different filler concentration can also be explained using percolation theory [53, 54] as shown in Fig. 8d. The experimental dielectric constant value at 500 Hz of the composite is fitted using the following power law equation, i.e.,

$$\varepsilon_{\text{eff}} \propto \varepsilon_{\text{m}} \left(f_{\text{c}} - f\right)^{-q}, \text{ for } f < f_{\text{c}} \tag{5}$$

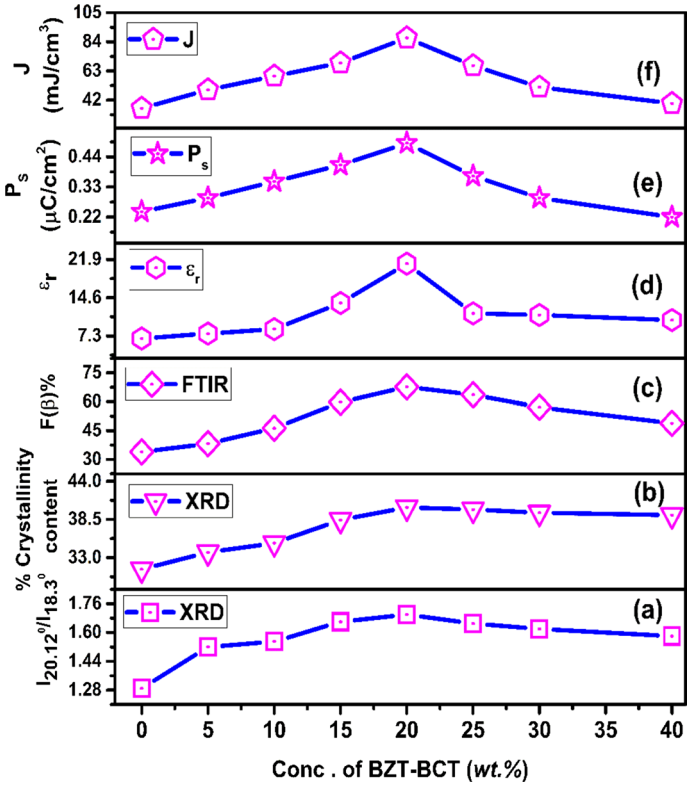

Fig. 9 (Color online) Variation of **a** $I_{20.12°}/I_{18.3°}$ **b** % of crystallinity **c** F(β)% d) ε_r **e** P_s **f** J of PVDF-HFP + ϕ wt% BZT-BCT polymer composites (ϕ = 0, 5, 10, 15, 20, 25, 30, 40)

where ε_{eff} and ε_m are the dielectric constant of the BZT-BCT/PVDF-HFP composites and PVDF-HFP matrix, respectively, f is the volume fraction of BZT-BCT particles, f_c is the percolation threshold which depends on the filler morphology and q is the critical exponent. The fitting parameters f_c and q obtained are 0.1953 and 0.29, respectively. The minimum volume content of filler where the percolation takes place named as percolation threshold, f_c. Here, the threshold value is found to be 19.53% around which an enhanced ε_r is obtained as seen from fitting the dielectric permittivity and it is close to experimental value, i.e., 20 wt%. Hence, in polymer–ceramic composites, f_c plays a vital role [54–56]. So, the interaction between surface charges of filler with the dipole of polymer plays an important role in the enhancement of β phase and it leads to enhancement of dielectric and ferroelectric properties.

The dielectric constant (ε_r) and saturation polarization (P_s) of composite depend on the physical properties of individual constituents, (filler and matrix), filler concentration, size and distribution of the dispersed filler in the host matrix which depends on the preparation technique [57]. Along with this, the interaction between filler and matrix affects electroactive β phase percentage which strongly

affects the physical properties [58–60]. So, we have plotted the change in crystallinity, β phase fraction (from XRD and FTIR), dielectric, ferroelectric properties and energy storage density with different filler concentration of BZT-BCT and is shown in Fig. 9. At lower filler concentration, a weak interaction occurs between filler and matrix and it results a lower value of $F(\beta)$ % due to which lower values of dielectric constant and saturation polarization is observed. With the increase in filler concentration, these values are enhanced up to 20 wt% due to the enhancement of β phase around which the highest ε_r, P_s and J has been observed. This signifies that there is a direct relationship between % of crystallinity, enhancement of β phase with the dielectric, ferroelectric properties and storage energy density.

Conclusion

Flexible polymer (PVDF-HFP)–ceramic (BZT-BCT) composites were successfully synthesized by solution casting technique. Structural and morphological studies revealed composite nature of the mixture. The electroactive β-phase of the polymer composite with 20 wt% filler concentration found to be 68%, double of that of pure PVDF-HFP. The interaction between polymer and ceramic is nothing but the 'dipole-surface charge' interaction and that resulted in the enhancement of β phase. The composite film with 20 wt% BZT-BCT ceramic exhibited an enhanced dielectric constant of 21 at 500 Hz which is three times more compared to the pure PVDF-HFP ($\varepsilon_r = 7$). Moreover, an improved polarization value of 0.5 μC/cm^2 was obtained in the composite film with 20 wt% BZT-BCT, which is more than double the polarization value of pure polymer. The maximum energy storage density of the composite reached to 86.85 mJ/cm^3 with 20 wt% of filler concentration at 300 kV/cm, which is double compared to the pure polymer matrix (36.08 mJ/cm^3). The improved dielectric and ferroelectric properties are well correlated with the enhancement of β phase. Further, the variations of the dielectric constant with filler concentration are also explained by percolation theory.

Acknowledgements Smaranika Dash acknowledges Ministry of Human Resource Development, India for the research fellowship. One of our Co- author, H.S.M. acknowledges Council of Scientific and Industrial Research (CSIR), India for the SRF fellowship.

References

1. Barick BK, Mishra KK, Arora AK, Choudhary RNP, Pradhan DK (2011) Impedance and Raman spectroscopic studies of $(Na_{0.5}Bi_{0.5})TiO_3$. J Phys D Appl Phys 44:355402
2. Mohanty HS, Dam T, Borkar H, Pradhan DK, Mishra KK, Kumar A, Sahoo B, Kulriya PK, Cazorla C, Scott JF, Pradhan DK (2019) Structural transformations and physical properties of $(1-x)$ $Na_{0.5}Bi_{0.5}TiO_3 - x$ $BaTiO_3$ solid solutions near a morphotropic phase boundary. J Phys: Condens Matter 31:075401
3. Kao KC (2004) Dielectric phenomena in solids. Elsevier Academic Pres, California
4. Yu K, Wang H, Zhou Y, Bai Y, Niu Y (2013) Enhanced dielectric properties of $BaTiO_3$/poly(vinylidene fluoride) nanocomposites for energy storage applications. J Appl Phys 113:034105

5. Prateek TV, Gupta RK (2016) Recent progress on ferroelectric polymer-based nanocomposites for high energy density capacitors: synthesis, dielectric properties, and future aspects. Chem Rev 116:4260–4317
6. Pfeifer S, Bandaru PR (2014) A methodology for quantitatively characterizing the dispersion of nanostructures in polymers and composites. Mater Res Lett 2:166–175
7. Jesson DA, Watts JF (2012) The interface and interphase in polymer matrix composites: effect on mechanical properties and methods for identification. Polym Rev 52:321–354
8. Liu S, Xue S, Zhang W, Zhai J, Chen G (2014) Significantly enhanced dielectric property in PVDF nanocomposites flexible films through a small loading of surface-hydroxylated $Ba_{0.6}Sr_{0.4}TiO_3$ nanotubes. J Mater Chem A 2:18040–18046
9. Feng Y, Li WL, Hou YF, Yu Y, Cao WP, Zhang TD, Fei WD (2015) Enhanced dielectric properties of PVDF-HFP/$BaTiO_3$-nanowire composites induced by interfacial polarization and wire-shape. J Mater Chem C 3:1250–1260
10. Bharath RS, Chakraborthy T, Nhalil H, Masin B, Ashok K, Sreemoolanadhan H, Oommena C, Elizabeth S (2019) Synthesis and evaluation of PVDF–$MgTiO_3$ polymer–ceramic composites for low-*k* dielectric applications. J Mater Chem C 7:4484–4496
11. Sousa RE, Pereira JN, Ferreira JCC, Costa CM, Machado AV, Silva MM, Mendez SL (2014) Microstructural variations of poly(vinylidene fluoride co-hexafluoropropylene) and their influence on the thermal, dielectric and piezoelectric properties. Polym Test 40:245–255
12. Wang C, Zhang J, Gong S, Ren K (2018) Significantly enhanced breakdown field for core-shell structured poly(vinylidene fluoride-hexafluoropropylene)/TiO_2 nanocomposite for ultra-high energy density capacitor applications. J Appl Phys 124:154103
13. Adhikary P, Mandal D (2017) Enhanced electro-active phase in a luminescent P(VDF–HFP)/Zn^{2+} flexible composite film for piezoelectric based energy harvesting applications and self-powered UV light detection. Phys Chem Chem Phys 19:17789–17798
14. Sultana A, Sadhukhan P, Alam MM, Das S, Middya TR, Mandal D (2018) Organo-lead halide perovskite induced electroactive β-phase in porous PVDF films: an excellent material for photoactive piezoelectric energy harvester and photodetector. Appl Mater Interfaces 10:4121–4130
15. Zhang S, Tong W, Wang J, Wang W, Wang Z, Zhang Y (2019) Modified sepiolite/PVDF-HFP composite film with enhanced piezoelectric and dielectric properties. J Appl Polym Sci 136:48412
16. Nakamura K, Sawai D, Watanabe Y, Taguchi D, Takahashi Y, Furukawa T, Kanamoto T (2003) Effect of annealing on the structure and properties of poly(vinylidene fluoride) β-form films. J Polym Sci B 41:1701–1712
17. Kumar RS, Sarathi T, Venkataraman KK, Bhattacharyya A (2019) Enhanced piezoelectric properties of polyvinylidene fluoride nanofibers using carbon nanofiber and electrical poling. Mater Lett 255:126515
18. Parangusan H, Ponnamma D, AlMaadeedb MAA (2018) Investigation on the effect of γ-irradiation on the dielectric and piezoelectric properties of stretchable PVDF/Fe–ZnO nanocomposites for self-powering devices. Soft Matter 14:8803–8813
19. Shepelin NA, Glushenkov AM, Lussini VC, Fox PJ, Dicinoski GW, Shapter JG, Ellis AV (2019) New developments in composites, copolymer technologies and processing techniques for flexible fluoropolymer piezoelectric generators for efficient energy harvesting. Energy Environ Sci 12:1143–1176
20. Kar E, Bose N, Das S, Mukherjee N, Mukherjee S (2015) Enhancement of electroactive β phase crystallization and dielectric constant of PVDF by incorporating GeO_2 and SiO_2 nanoparticles. Phys Chem Chem Phys 17:22784–22798
21. Spitalsky Z, Tasis D, Papagelis K, Galiotis C (2010) Carbon nanotube–polymer composites: chemistry, processing, mechanical and electrical properties. Prog Polym Sci 35:357–401
22. Liu YL, Li Y, Xu JT, Fan ZQ (2010) Cooperative effect of electrospinning and nanoclay on formation of polar crystalline phases in poly(vinylidene fluoride). Appl Mater Interfaces 2:1759–1768
23. Yuan JK, Li WL, Yao SH, Lin YQ, Sylvestre A, Bai J (2011) High dielectric permittivity and low percolation threshold in polymer composites based on SiC-carbon nanotubes micro/nano hybrid Appl. Phys Lett 98:032901
24. Dang ZM, Yuan JK, Zha JW, Zhou T, Li ST, Hu GH (2012) Fundamentals, processes and applications of high-permittivity polymer–matrix composites. Prog Mater Sci 57:660–723
25. Luo B, Wang X, Wang Y, Li L (2014) Fabrication, characterization, properties and theoretical analysis of ceramic/PVDF composite flexible films with high dielectric constant and low dielectric loss. J Mater Chem A 2:510–519

26. Harstad S, Dsouza N, Soin N, Gendy AAE, Gupta S, Pecharsky VK, Shah T, Siores E, Hadimani RL (2017) Enhancement of β-phase in PVDF films embedded with ferromagnetic Gd_5Si_4 nanoparticles for piezoelectric energy harvesting. AIP Adv A 7:056411
27. Jain A, Prashanth KJ, Sharma AK, Jain A, Rashmi PN (2015) Dielectric and piezoelectric properties of PVDF/PZT composites: a review. Polym Eng Sci 55:1589–1616
28. Liu W, Ren X (2009) Large piezoelectric effect in Pb-free ceramics. Phys Rev Lett 103:1257602
29. Kumar P, Mishra P, Sonia S (2013) Synthesis and characterization of lead-free ferroelectric $0.5[Ba(Zr_{0.2}Ti_{0.8})O_3]$–$0.5[(Ba_{0.7}Ca_{0.3})TiO_3]$—polyvinylidene difluoride 0–3 composites. J Inorg Organomet Polym 23:539–545
30. Sadhu SPP, Siddabattuni S, Muthukumar VS, Varma KBR (2018) Enhanced dielectric properties and energy storage density of surface engineered BCZT/PVDF-HFP nanodielectrics. J Mater Sci: Mater Electron 29:6174–6182
31. Dash S, Mohanty HS, Bhoi K, Kant R, Kumar A, Thomas R, Pradhan DK (2018) Sintering dependent Ca^{2+} solubility in barium titanate synthesized by sol–gel auto combustion method. J Mater Sci: Mater Electron 29:20820–20831
32. Coondoo I, Panwar N, Amorın H, Alguero M, Kholkin AL (2013) Synthesis and characterization of lead-free $0.5Ba(Zr_{0.2}Ti_{0.8})O_3$-$0.5(Ba_{0.7}Ca_{0.3})TiO_3$ ceramic. J Appl Phys 113:214107
33. Tian Y, Wei L, Chao X, Liu Z, Yang Z (2013) Phase transition behavior and large piezoelectricity near the morphotropic phase boundary of lead-free (Ba0.85Ca0.15)(Zr0.1Ti0.9)O3 ceramics. J Am Ceram Soc 96:496–502
34. Ma W, Zhang J, Chen S, Wang X (2008) β-Phase of poly(vinylidene fluoride) formation in poly(vinylidene fluoride)/poly(methyl methacrylate) blend from solutions. Appl Surf Sci 254:5635–5642
35. Wright DGM, Dunk R (1988) The effect of crystallinity on the properties of injection moulded polypropylene and polyacetal. Polymer 29:793–796
36. Nalwa HS (1995) Ferroelectric polymers: chemistry, physics and applications 28, Hudgin DE. Marcel Dekker, Inc., New York
37. Bryant WMD, Pierce RHH, Lindegren CR, Roberts R (1955) Nucleation and growth of crystallites in high polymers. Formation of spherulites. J Polym Sci 16:131–142
38. Pethrick RA (2007) Polymer structure characterization: from nano to macro organization. RSC Publishing, New York
39. Palza H, Vera J, Wilhelm M, Zapata P (2011) Spherulite growth rate in polypropylene/silica nanoparticle composites: effect of particle morphology and compatibilizer. Macromol Mater Eng 296:744–751
40. Dutta B, Kar E, Bose N, Mukherjee S (2015) Significant enhancement of the electroactive β-phase of PVDF by incorporating hydrothermally synthesized copper oxide nanoparticles. RSC Adv 5:105422–105434
41. Mishra P, Kumar P (2015) Structural, dielectric and optical properties of [(BZT–BCT)-(epoxy-CCTO)] composites. Ceram Int 41:2727–2734
42. Mehto VR, Rathore D, Pandey RK (2014) Optical and structural properties of electrodeposited polyaniline/Q-CdS composites. Polym Comput 35:1864–1874
43. Wood DL, Tauc J (1972) Weak absorption tails in amorphous semiconductors. Phys Rev B 5:3144–3151
44. Rani J, Yadav KL, Prakash S (2014) Structural, dielectric and optical properties of sol–gel synthesized $0.55Ba(Zr_{0.2}Ti_{0.8})O_3$–$0.45(Ba_{0.7}Ca_{0.3})TiO_3$ ceramic. Appl Phys A 117:1131–1137
45. Aziz SB, Abdullah OG, Rasheed MA (2017) A novel polymer composite with a small optical band gap: new approaches for photonics and optoelectronics. J Appl Polym Sci 134:44847
46. Cavalcante LS, Marques VS, Sczancoski JC, Escote MT, Joya MR, Varela JA, Santos MRMC, Pizani PS, Longo E (2008) Synthesis, structural refinement and optical behavior of $CaTiO_3$ powders: a comparative study of processing in different furnaces. Chem Eng J 143:299–307
47. Araujo MM, Silva LKR, Sczancoski JC, Orlandi MO, Longo E, Santos AGD, Sa JLS, Santos RS, Luz GE, Cavalcante LS (2016) Anatase TiO_2 nanocrystal anchored at inside of SBA-15 mesopores and their optical behavior. Appl Surf Sci 389:1137–1147
48. Yu L, Cebe P (2009) Crystal polymorphism in electrospun composite nanofibers of poly(vinylidene fluoride) with nanoclay. Polymer 50:2133–2141
49. Shanthi PM, Hanumantha PJ, Albuquerque T, Gattu B, Kumta PN (2018) Novel composite polymer electrolytes of PVdF-HFP derived by electrospinning with enhanced Li-ion conductivities for rechargeable lithium-sulfur batteries. Appl Energy Mater 1:483–494

50. Frank SC (1968) Waves: Berkeley physics course, vol 3. McGraw-Hill book company, New York
51. Patra A, Pal A, Sen S (2018) Polyvinylpyrrolidone modified barium zirconate titanate/polyvinylidene fluoride nanocomposites as self-powered sensor. Ceram Int 44:11196–11203
52. Dan Yu, Nuo-xin X, Liang H, Zhang Q-l, Yang H (2015) Nanocomposites with $BaTiO_3$–$SrTiO_3$ hybrid fillers exhibiting enhanced dielectric behaviours and energy-storage densities. J Mater Chem C 3:4016–4022
53. He F, Lau S, Chan HL (2009) High dielectric permittivity and low percolation threshold in nanocomposites based on poly(vinylidene fluoride) and exfoliated graphite nanoplates. Adv Mater 21:710–715
54. Chen Q, Du P, Jin L, Weng W, Han G (2007) Percolative conductor/polymer composite films with significant dielectric properties. Appl Phys Lett 91:022912
55. Dahiya HS, Kishore N, Mehra RM (2007) Effect of percolation on electrical and dielectric properties of acrylonitrile butadiene styrene/graphite composite. J Appl Polym Sci 106:2101–2110
56. Jia Q, Huang X, Wang G, Diao J, Jiang P (2016) MoS_2 nanosheet superstructures based polymer composites for high-dielectric and electrical energy storage applications. J Phys Chem C 120:10206–10214
57. Harito C, Bavykin DV, Yuliarto B, Dipojono HK, Walsh FC (2019) Polymer nanocomposites having a high filler content: synthesis, structures, properties, and applications. Nanoscale 11:4653–4682
58. Hu T, Juuti J, Jantunen H, Vilkman T (2007) Dielectric properties of BST/polymer composite. J Eur Ceram Soc 27:3997–4001
59. Mohanty HS, Ravikant KA, Kurliya PK, Thomas R, Pradhan DK (2019) Dielectric/ferroelectric properties of ferroelectric ceramic dispersed poly(vinylidene fluoride) with enhanced β-phase formation. Mater Chem Phys 230:221–230
60. Mohanty HS, Sharma SK, Ravikant KP, Kumar A, Thomas R, Pradhan DK (2019) Enhanced functional properties of soft polymer-ceramic composites by swift heavy ion irradiation. Phys Chem Chem Phys 21:24629–24642

Affiliations

Smaranika Dash[1] · Hari Sankar Mohanty[1] · Ravikant[2,3,4] · Ashok Kumar[2,3] · Reji Thomas[5,6] · Dillip K. Pradhan[1]

1 Department of Physics and Astronomy, National Institute of Technology, Rourkela, Odisha 769008, India

2 CSIR-National Physical Laboratory, Dr. K.S. Krishnan Marg, New Delhi 110012, India

3 Academy of Scientific and Innovative Research (AcSIR), Ghaziabad 201002, India

4 Department of Physics, Government College Sailana, Vikram University, Ujjain, Madhya Pradesh 456010, India

5 Division of Research and Development, Lovely Professional University, Jalandhar-Delhi G.T. Road, Phagwara, Punjab 144411, India

6 School of Chemical Engineering and Physical Sciences, Lovely Professional University, Jalandhar-Delhi G.T. Road, Phagwara, Punjab 144411, India